UNIVERSIDADE DE SANTIAGO DE COMPOSTELA

FACULTADE DE FÍSICA
Departamento de Física de Partículas
Grupo Experimental de Núcleos y Partículas

Characterization of the ALADIN setup at GSI for Coulomb Dissociation experiments

Traballo de Investigación Tutelado
dirixido por:
Dr. Dolores Cortina Gil
e presentado por:
Carme Rodríguez Tajes
para a obtención do
Diploma de Estudos Avanzados
Setembro 2006

Caracterization of the ALADIN setup at GSI for Coulomb Dissociation experiments

Carme Rodríguez Tajes

September 2006

Contents

List of Figures

List of Tables

Introduction

One of the most important objectives in nuclear astrophysics is the description of the thermonuclear reactions asociated with the energy production and the nucleosynthesis in the stars.

In hot and dense stellar environments such as novae, the main nuclear energy source is explosive hydrogen burning, which occurs as a series of particle captures and β decays of radioactive isotopes (see rp process in figure 1). The competition between both kind of reactions determines the path followed by the process. Detailed measurements of low energy capture reactions involved in the process are required to fully understand it [1].

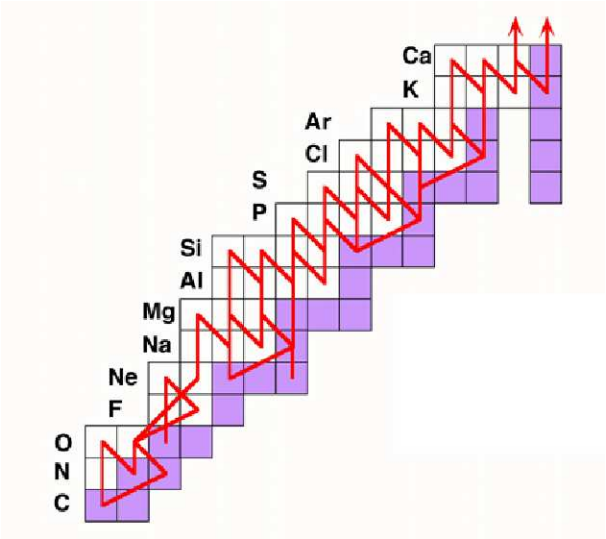

Figure 1: *rp-process burning in an energetic novae, Champagne and Wiescher (1992).*

The nucleosynthesis of long lived radioactive isotopes is specially interesting, as they can be observed with γ-ray observatories as INTEGRAL [2] or COMPTEL [3]. This is the case of the nucleus ^{22}Na, produced in Ne novae stars via the sequence $^{20}Ne(p,\gamma)^{21}Na(p,\gamma)^{22}Mg(\beta^{+}\nu)^{22}Na$. However, the attemps of observing the 1.275 MeV γ-ray following the decay of ^{22}Na only yielded to an upper limit on its production, which is below the theoretical predictions [4]. The proton capture $^{22}Mg(p,\gamma)^{23}Al$ could be an escape reaction from this chain and lead to the synthesis of heavier nuclei, resulting in a reduction of the ^{22}Na abundance. An accurate measurement of this reaction rate is necessary to estimate the ^{22}Na production and constitutes one of the few experimental cases that makes a comparison with γ-ray observation possible.

The mechanism of the $^{22}Mg(p,\gamma)^{23}Al$ reaction is one proton capture feeding directly the ground state of ^{23}Al or the resonant capture through the ^{23}Al excited states. In the astrophysical environment, the resonant capture through the first excited state would dominate the process because its location, 405 KeV above the proton threshold, it is near the Gamow energy in typical explosive burning conditions (200 $KeV - 650$ KeV).

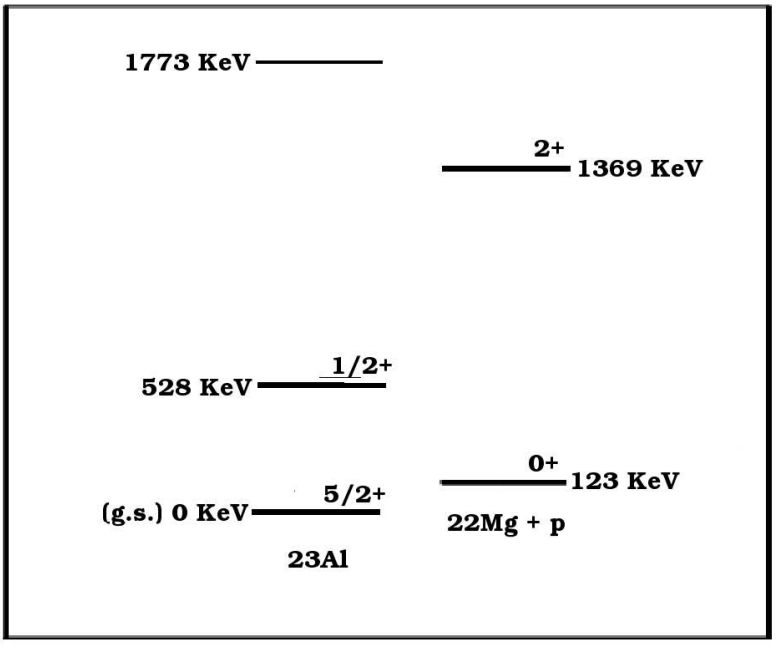

Figure 2: *Energy level schemes of* ^{23}Al *[5] and* ^{22}Mg.

In order to study radioactive proton capture reactions of astrophysical interest, we will have to solve some experimental difficulties by selecting an appropiate technique. One possibility consists on sending a proton beam on a target, that in our case would be unstable. However, the use of radioactive targets is only posible when we work with long lived nuclei. Another possibility consists on sending radioactive beams, in inverse kinematics, on a proton target. But in this case the presence of the coulomb barrier reduces drastically the cross section of the reaction when they are studied at lower energies. Both methods are known as direct measurements.

The coulomb dissociation technique is an alternative method to the direct measurement of capture reactions. It was first proposed in 1986 by Baur, Bertulani and Rebel based on the semi-clasical virtual photon theory [6]. We use the residual nucleus B from the process $A(X,\gamma)B$ and we make it interact with the electromagnetic field induced by a target with high atomic number. The nucleus B goes to an excited state and decays to $A+X$. The electromagnetic interaction was described by the equivalent virtual photon method, where the effect of the electromagnetic field is equal to the effect of certain light pulses called virtual photons.

The process of absorbing a virtual photon $B(\gamma,X)A$ corresponds to the inverse of the proton capture reaction. Taking this into account, the two cross sections are related and we can calculate the one by measuring the other.

The coulomb dissociation (CD) technique has two main advantages, it makes possible the use of stable targets and the cross sections involved, in the order of *mbarn*, are aproximately three times larger than most of the direct capture cross sections.

The next year it is planned to measure at GSI (Darmstadt) [7] the coulomb dissociation reaction $^{208}Pb(^{23}Al,^{22}Mg+p)^{208}Pb$ with the objetive of studying the radioactive proton capture $^{22}Mg(p,\gamma)^{23}Al$. The experiment will take place at the ALADIN setup, being the first time that it is used for this kind of measurement.

In figure 3 we show the GSI facility. The unstable nuclei ^{23}Al will be obtained by nuclear fragmentation of a primary beam, previously acelerated in the SIS syncrotron, in a production target located at the entrance of the Fragment Separator (FRS). They will be selected by the $B\rho-\Delta E-B\rho$ technique in the FRS.

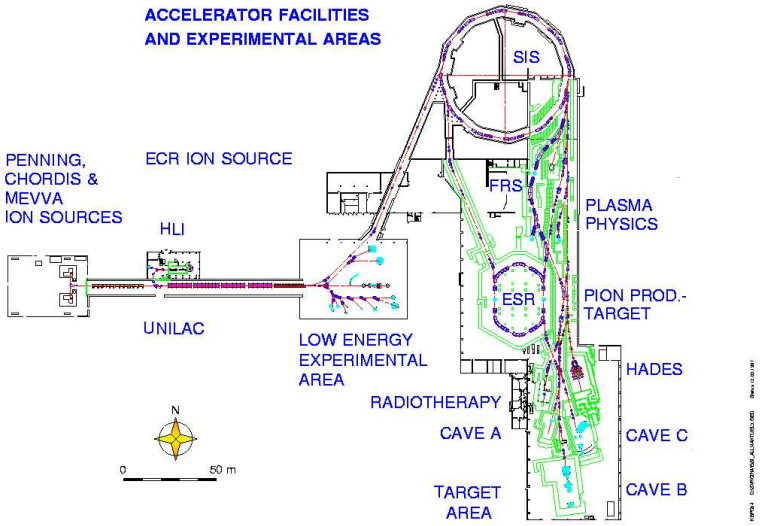

Figure 3: *Gesellschaft für Schwerionenforschung (GSI) facility, Darmstadt (Deutschland).*

Then, the ^{23}Al secondary beam will be transmitted to the ALADIN setup, placed in the cave C of the SIS experimental area. The nuclei will interact with the electromagnetic field induced by a ^{208}Pb target, resulting an excited state which will decay to $^{22}Mg + p$.

The reaction fragments will be analyzed by means of the ALADIN dipole and a set of tracking detectors that would allow the determination of the invariant mass and the scattering angle of the reaction.

Our work is focused on the experiment preparation and it can be divided into two parts. The aim of the first one is to fix the experimental setup, this means to decide on the optimum energy of the reaction, the thickness of the Pb target and the location of the tracking detectors. For this purpose, we have performed a realistic simulation of the coulomb dissociation fragments in the ALADIN setup with the software package Geant 3.21.

The second part of the work is dedicated to develope a flexible method for the momentum reconstruction of the produced protons, needed to determine the relative energy between the CD fragments and the scattering angle of the reaction.

The momentum distribution of the ^{22}Mg ions is expected to be very narrow and centered in the value corresponding to the secondary beam energy. This allows us to use the momentum asociated with the beam energy for the ^{22}Mg without introducing a significant error. In this case, the proton momentum will be the most important parameter for the determination of the relative energy and the scattering angle. It will be calculated from the registered positions in the tracking detectors, placed before and after the ALADIN dipole.

Furthermore, many other experiments are planned in the Cave C with the same experimental setup proposed for the ^{23}Al coulomb dissociation. The developed work will be also a help in their preparation.

Chapter 1

The simulations

1.1 Software used for the simulations

We performed the simulations needed for our study with the software package Geant 3.21 [8]. We introduced some modifications to improve the description of the interaction of the ions with the matter [9]. We conserved the Geant 3.21 estimations for the angular straggling; but we calculated the energy loss and the energy straggling with the AMADEUS subroutines [10][11], which provide results in good agreement with the avaliable experimental data and with the ATIMA [12] estimations. As the code was originally created to work with light particles, these corrections are more relevant when we consider heavy ions.

The package Geant 3.21 simulates the track of an ion within a layer of matter by dividing it into steps with a certain size. The code calculates the energy loss and the angular deviation for each step and it updates the energy, the momentum and the position of the ion. In principle, the step size can be automatically chosen by Geant, taking into account the characteristics of the media.

However, we found that for light media this option leads to some errors in the simulation because the automatic step size can be too big. For instance, although the magnitude of the angular straggling is always well calculated, its effect over the position of the ion will not be well reproduced because the angular deviation will be applied only in the next step. In order to avoid these problems, we fixed the maximum step size to 0.1 cm when an accurate simulation was required.

We tried to develope a simulation which could be easily used by different people. The most important parameters of the simulation as the event generator, the energy of the ions, the emission point, the geometric option or the magnetic field are selected just by changing an external input file without need to compile the code again.

1.2 Simulated ALADIN setup

The simulated setup is surrounded by air. It is basically composed by a *Pb* target, the ALADIN dipole and a set of tracking detectors placed before and after the magnet which will allow us to calculate the emission angles of the CD fragments and the proton momentum; i.e., the magnitudes needed to determine the invariant mass and the scattering angle of the reaction.

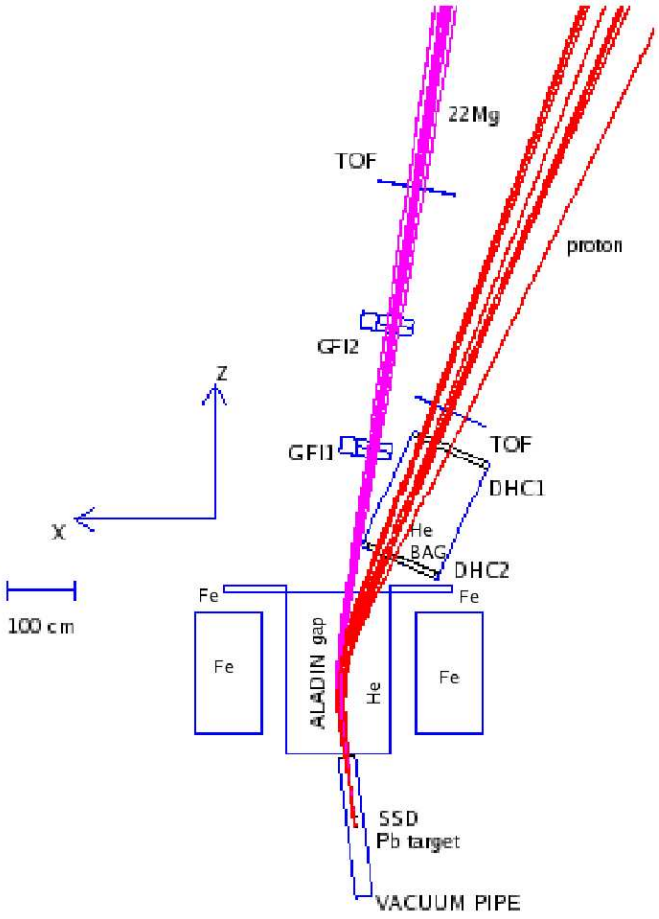

Figure 1.1: ^{23}*Al coulomb dissociation fragments in the simulated ALADIN setup.*

We show in figure 1.1 the simulated setup, where the following elements are taken into account

1. We have a vaccuum pipe which goes up to the entrance of the magnet, with a 250 μm iron exit window. This pipe follows the beam line and it is rotated 7.2 deg respect to the dipole z axis.

2. Within the vacuum pipe, there is a Pb target, where the coulomb dissociation reaction takes place. We have a silicon multistrip detector (SSD) behind it to measure the (x, y) position of the produced fragments. The characteristics of the detector are summarized in table 1.1.

Active area $x \times y$ (cm)	$7. \times 4.$
Media	Si
Thickness (cm), (mg/cm^2)	0.03, 69.9
Spatial resolution, σ (cm)	0.003

Table 1.1: *Characteristics of the silicon multistrip detector*

In the real experiment, we will track the ^{23}Al beam before the target. This tracking will allow to determine the reaction point in the target and to calculate the emission angles (θ and ϕ) of the CD products following the equations 1.1 and 1.2, where $L = 15$ cm is the distance between the Pb target and the silicon detector.

$$\theta = atan\frac{\sqrt{(x_{SSD} - x_{target})^2 + (y_{SSD} - y_{target})^2}}{L} \tag{1.1}$$

$$\phi = \begin{cases} atan\frac{y_{SSD}-y_{target}}{x_{SSD}-x_{target}} & x_{SSD} > x_{target} \text{ and } y_{SSD} \geq y_{target} \\ atan\frac{y_{SSD}-y_{target}}{x_{SSD}-x_{target}} + \pi & x_{SSD} \leq x_{target} \text{ and } y_{SSD} > y_{target} \\ atan\frac{y_{SSD}-y_{target}}{x_{SSD}-x_{target}}) + \pi & x_{SSD} \leq x_{target} \text{ and } y_{SSD} \leq y_{target} \\ atan\frac{y_{SSD}-y_{target}}{x_{SSD}-x_{target}}) + 2\pi & x_{SSD} > x_{target} \text{ and } y_{SSD} \leq y_{target} \end{cases} \tag{1.2}$$

In our work, we did not consider the ^{23}Al beam and we only simulated the emitted CD fragments. This means that the reaction point is for us the emission point of the ^{22}Mg and the proton. We do not take into account the limited resolution due to the reconstruction of the reaction point. This factor should be included in the future in order to have a more realistic simulation.

3. We have also simulated the gap of the ALADIN dipole ($155. \times 50. \times 230.\ cm$) filled with He in order to reduce the angular straggling. The iron constraints of the magnet have been also included in the simulation.

4. We have also considered two different branches for the two CD fragments, composed by tracking detectors and a TOF wall. They follow respectively the trajectories of the ^{22}Mg ions and protons, the first one is rotated 9.2 deg respect to the z axis of the dipole and the second one, 21.5 deg.

5. The tracking detectors placed after the magnet are two GFI detectors for the ^{22}Mg ions and two drift chambers (DHC) for the protons. Their characteristics are given in tables 1.2 and 1.3.

Active area $x \times y$ (cm)	$50. \times 50.$
Media	*Scintillator plastic* C_9H_{10}
Thickness (cm), (mg/cm^2)	0.1, 103.2
Spatial resolution, σ (cm)	0.1

Table 1.2: *Characteristics of the GFI detectors.*

Active area $x \times y$ (cm)	102.8×80.4
Media	$50\%\ Ar + 50\%\ C_2H_6$
Thickness (cm), (mg/cm^2)	$8., 8.$
Spatial resolution, σ (cm)	0.02

Table 1.3: *Characteristics of the drift chambers*

We have also included Al frames for these detectors and two 12 μm mylar layers for each DHC, limiting the active volume. The drift chambers for protons are placed as close as posible to the magnet in order to optimize the geometric efficiency.

6. We have introduced an He bag between both DHC to reduce the angular straggling suffered by the protons in the air surrounding the setup. The bag is separated from the outside media by 12 μm mylar layers located at the entrance and the at exit of the volume.

7. Finally, two TOF detectors have been included. The TOF wall for the protons will be used in the experiment only as trigger whereas the one for the ^{22}Mg will provide an aditional identification of the ions by measuring their velocities. In principle, the identification of the ^{22}Mg ions will be done by means of the energy loss in the silicon detector, but as this measurement is not expected to be accurate enough, they will be also identified using the TOF technique.

In the external input file of the simulation we can choose between different geometric options. The one explained above reproduces the real experimental situation, but there are some other avaliable options which we used in the proton momentum reconstruction. We will explain them in the next chapter.

1.3 Magnetic field of the ALADIN dipole

The magnetic field used in the simulation comes from measured maps avaliable at GSI. We used a field map where the x, y and z dimensions of the magnet were covered by intervals of 5 cm. Our code gets the magnetic field value for a given point $\vec{r_0} = (x_0,\ y_0,\ z_0)$ within the magnet by an interpolation in the mentioned map, using the equation 1.3.

$$\begin{aligned} B_i(\vec{r_0}) &= (1-t)(1-u)(1-v)B_i(\vec{r_1}) \\ &+ (1-u)(1-v)B_i(\vec{r_2}) \\ &+ tu(1-v)B_i(\vec{r_3}) \\ &+ tuvB_i(\vec{r_4}) \\ &+ (1-t)u(1-v)B_i(\vec{r_5}) \\ &+ (1-t)uvB_i(\vec{r_6}) \\ &+ (1-t)(1-u)vB_i(\vec{r_7}) \\ &+ t(1-u)vB_i(\vec{r_8}) \quad i = x,\ y\ z \end{aligned} \tag{1.3}$$

where

$$\begin{aligned} t &= \frac{x_0 - x_{lt}}{x_{gt} - x_{lt}} \\ u &= \frac{y_0 - y_{lt}}{y_{gt} - y_{lt}} \\ v &= \frac{z_0 - z_{lt}}{z_{gt} - z_{lt}} \end{aligned} \tag{1.4}$$

and

$$\begin{aligned}
\vec{r_1} &= (x_{lt},\ y_{lt},\ z_{lt}) \\
\vec{r_2} &= (x_{gt},\ y_{lt},\ z_{lt}) \\
\vec{r_3} &= (x_{gt},\ y_{gt},\ z_{lt}) \\
\vec{r_4} &= (x_{gt},\ y_{gt},\ z_{gt}) \\
\vec{r_5} &= (x_{lt},\ y_{gt},\ z_{lt}) \\
\vec{r_6} &= (x_{lt},\ y_{gt},\ z_{gt}) \\
\vec{r_7} &= (x_{lt},\ y_{lt},\ z_{gt}) \\
\vec{r_8} &= (x_{gt},\ y_{lt},\ z_{gt})
\end{aligned}$$

The subscripts gt and lt make reference to the values of x, y and z in the field map which are next to x_0, y_0 and z_0, being $x_{lt} < x_0 < x_{gt}$, $y_{lt} < y_0 < y_{gt}$ and $z_{lt} < z_0 < z_{gt}$.

In figure 1.2 we plot the components of the magnetic field for a current of 1100 A. We can see that the most important one is the vertical B_y component of the field, which is constant along the x, y and z directions and responsible of the dipolar behavoir of the magnet. The B_x component of the field is neglectable and B_z is antisimmetric in the y and z coordinates. Taking this into account, the most relevant effect of the magnetic field over the ion trajectories will be a deflection in the x direction, depending on the ion and its energy as it is shown in equation 1.5, where m is the rest mass of the ion, q is its charge and ρ is the radio of curvature in the magnetic field B. We will use this effect to reconstruct the proton momentum.

$$\rho = \frac{\gamma m v}{B q} \tag{1.5}$$

It is clear that a bigger deflection will result in a better separation of the proton trajectories with different momentum and will improve the resolution in the momentum reconstruction. We have selected for the simulations the maximum intensity of the field that allowed the transmission of the protons, without hitting the magnet side walls. We see in equation 1.5 that the magnitude of the field has to be modified each time we consider a different energy in order to preserve the deflection power.

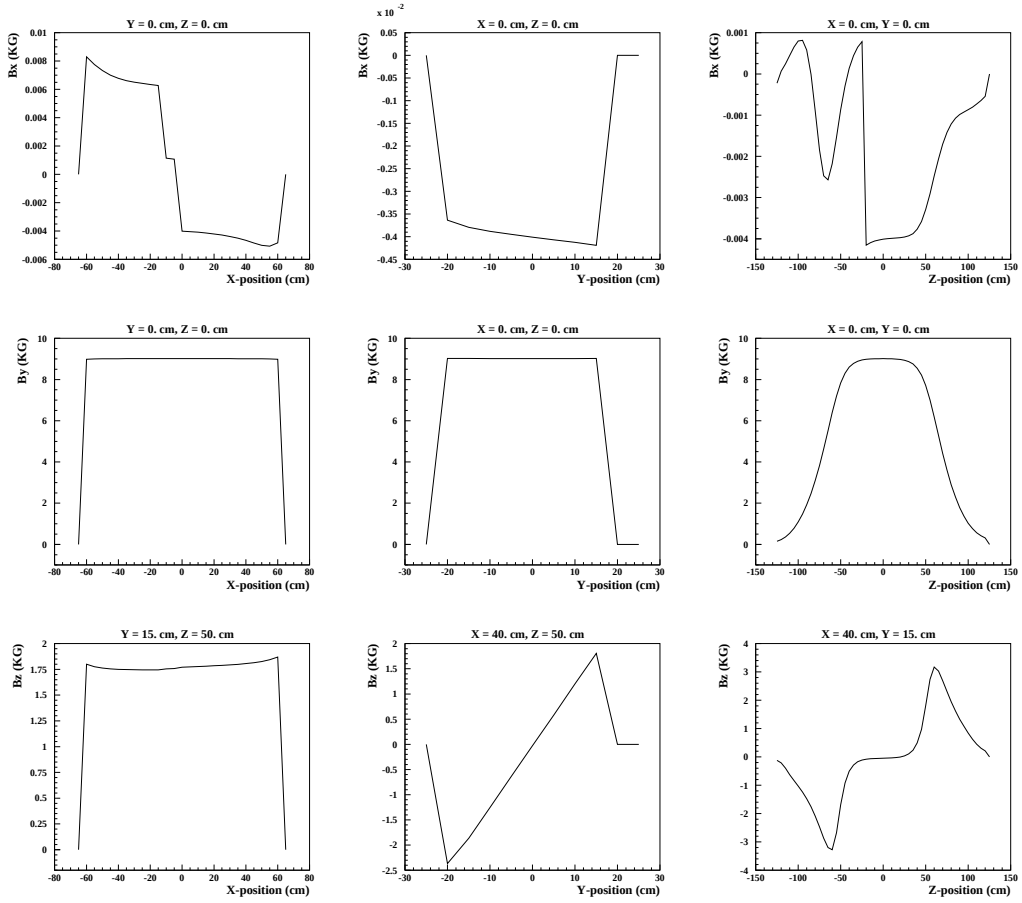

Figure 1.2: *Spatial behavoir of the ALADIN magnetic field components.*

We can select in the simulation the magnetic field, just modifying the external input file. The avaliable options are the following

1. ALADIN measured magnetic field.
2. Constant magnetic field in the y direction.
3. No field.

1.4 Event generators

We have used four different event generators. They allowed to simulate the CD fragments traversing the ALADIN setup or simply the proton momentum reconstruction.

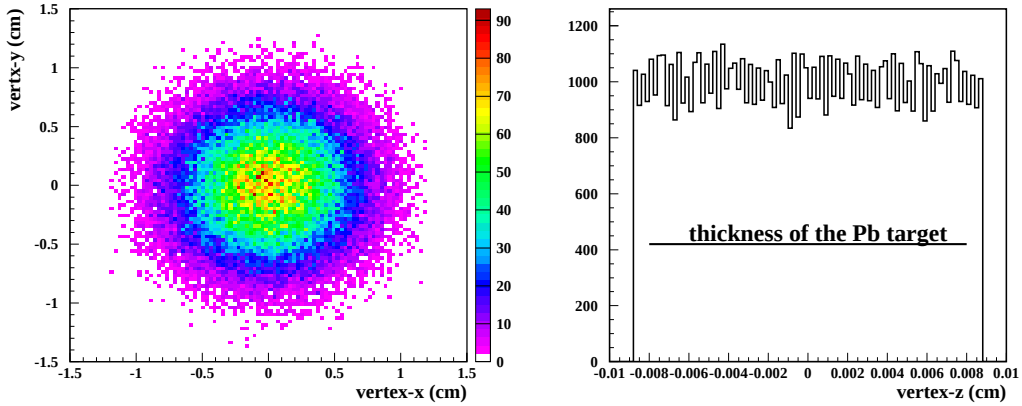

Figure 1.3: *Emission point of the coulomb dissociation fragments. We considered a* 200 mg/cm^2 *Pb target.*

The first case corresponds to a realistic simulation. The emission point within the target was forced to follow a gaussian distribution with $FWHM = 1\ cm$ in the x and y coordinates, reproducing the expected beam profile. For the z coordinate, the location straggling was taken into account by means of a step function covering the thickness of the Pb target (see figure 1.3).

We will introduce here the two event generators corresponding to this realistic case

1. *Transport of an ion through the setup*
   We have simulated ions with a given energy and emitted from the target with a certain angular aperture and energy spread.

   We have used this event generator for developing and testing our methods for the proton momentum reconstruction and we have simulated the behavoir of the protons coming out from the ^{23}Al CD reaction. We have followed the proton distributions in the ^{23}Al CD at 250 MeV/u, with an angular aperture of 0.02 rad and 20 MeV of energy spread.

2. ^{23}Al *coulomb dissociation*
   In this case, we have simulated the ^{22}Mg and the proton coming out from the ^{23}Al CD through the ALADIN setup.

The event generator is based on a data file where the 4-momentum of the proton and of the ^{22}Mg are stored for 10^5 CD events, which can be sequentially or randomly triggered. Due to the file structure, in the first case all the 10^5 events should be simulated in order to have a good description of the relative energy and scattering angle distributions. In the random case, we can trigger the number of events we want.

We have two different data files for the simulation of the ^{23}Al CD at 250 MeV/u and at 500 MeV/u. In both cases, only the excitation from the ^{23}Al ground state with a core spin of 0^+ for ^{22}Mg is considered.

There is also a third data file where we consider the posibility of feeding the first excited state 2^+ in ^{22}Mg from the ^{23}Al second excited state. This file is only avaliable for a CD reaction at 500 MeV/u.

The other two event generators correspond to the proton momentum reconstruction and they will be presented in the next chapter.

The simulation input file allows to choose between these four event generators. For the CD case (case 2), the corresponding data file with the 4-momentum of the fragments should be specified together with the selected triggering option.

Chapter 2

Proton momentum reconstruction

One of the goals of this work was to fix the setup for the ^{23}Al CD experiment together with the optimum energy for the reaction and the Pb target thickness. In this sense, we needed to study how the proton momentum resolution depends on the energy and on the angular straggling through the different layers of matter in the setup. In order to perform such a study we were pushed to develope a fast and flexible method for the proton momentum reconstruction.

For this purpose we used a simple event generator which allows us to consider the transport of protons through the ALADIN setup. In order to have a realistic simulation of the protons, we took into account the energy loss, the energy straggling and the angular straggling and we also included the finite resolution of the tracking detectors. The coordinates of the emission point within the target were forced to follow the expected distribution of the CD reaction point, already explained in the previous chapter.

For each one of the simulated trajectories, we stored in a file the coordinates of the emission point, the positions registered in the tracking detectors and the proton momentum. The structure of the file is shown in 2.1, where the suscript 0 makes reference to the emission point.

$$x_0,\ y_0,\ z_0,\ x_{SSD},\ y_{SSD},\ z_{SSD},\ x_{DHC1},\ y_{DHC1},\ z_{DHC1},\ x_{DHC2},\ y_{DHC2},\ z_{DHC2},\ P_{real} \tag{2.1}$$

These will be for us the *simulated measured protons*. We reconstruct the proton momentum by means of the positions in the detectors. The comparison of this determined momentum with the real one, P_{real}, allows to evaluate the reconstruction resolution.

2.1 Momentum reconstruction methods

We can univocally relate the ion momentum and its trajectory through the setup, knowing three points of the trajectory [13]

1. One point before the magnet and two points after the magnet.
2. Two points before the magnet and one point after the magnet.

Both ways are possible because we will measure two points before and after the ALADIN dipole. In particular, the tracking of the ^{23}Al beam will provide the emission point within the target and we will also have the position measurements of the silicon detector and the drift chambers.

We proposed two methods of reconstruction based on this principle, called respectively *forward tracking* and *backward tracking*. For both cases, we used a different Geant simulation (see section 3.2). The corresponding event generators use as input the file obtained from the proton realistic simulation; i.e., the file where we stored the positions and the momentum of the simulated measured protons (see equation 2.1).

We will simulate several proton trajectories trying to find the momentum which reproduces the measured positions for each measured proton given as input.

2.1.1 Momentum reconstruction by forward tracking

We simulate protons from the measured position in the target [1] and with emission angles θ and ϕ calculated from the point in the target and the position measurement

[1] Remind that we work with an infinite resolution for the determination of the x and y coordinates in the target (section 2.2). The z coordinate always corresponds to the center of the target.

Example 3.1:
Calculation of the proton momentum for a mean energy of 250 MeV

```
*.................................................1st iteration
IF(niter.eq.1)THEN
   p0 = 0.73 !GeV/c
   highp = 0.85 !GeV/c
   lowp = 0.61 !GeV/c

*.........................Look for the momentum which reproduces
*.........................the position "measured" by the 1st DHC
ELSE
   if(xdhc1_simulated.gt.xdhc1_measured)then
     highp = p0
   elseif(xdhc1_simulated.lt.xdhc1_measured)then
     lowp = p0
   endif
   p0 = lowp + 0.5*(highp-lowp)

*.............................................................
ENDIF
```

in the silicon detector, see equations 1.1 and 1.2. We look for the momentum which reproduces the x position measured by the first drift chamber, using the fact that larger values of x after the magnet mean a smaller deflection and a bigger momentum (and the opposite).

The example 3.1 shows the code we employed to define the momentum for each simulated trajectory. In the first simulated trajectory (first iteration) the proton momentum $p0$ will be always the one corresponding to the mean energy we are considering, for instance 250 MeV for the ^{23}Al CD at 250 MeV/u. We also define a maximum and a minimum initial momentum, *highp* and *lowp*, which correspond to the extremes of the expected proton momentum distribution.

In the next iteration, we compare the position obtained in the first drift chamber for the first simulated trajectory with the measured one. We evaluate whether it is larger or smaller and we redefine the values of *highp* or *lowp*, with them we calculate

Notice that this parameter will not be well determined in the experiment and it will not be used a measured value.

the momentum $p0$ for the next track.

The process continues until the convergency is achieved. In our case, this means that we get a position in the drift chamber closer than 100 μm to the measured one.

2.1.2 Momentum reconstruction by backward tracking

The idea is the same as in the previous case, but we invert the direction of the trajectories and the sign of the magnetic field. We simulate protons fixing the emission point to the position measured by the second drift chamber and the emission θ and ϕ angles to the ones calculated from the measurements in the two DHC. We look for the momentum which reproduces the position in the target, using the same convergency criteria as before; i.e., the x coordinate in the target we obtain for the simulated trajectory should be closer than 100 μm to the x value we have for the measured proton.

We made also some tests performing the backward tracking to the silicon detector and not to the target. We did not find any significant difference in the momentum resolution.

2.2 Simulations for the proton momentum reconstruction

The Geant simulations used for the proton momentum reconstruction are a bit different from the ones explained in the second chapter. The main differences, in the event generators, were already explained in the previous section but some others should be mentioned.

1. *Geometry*
   In the case of the reconstruction by forward tracking, we increased the x and y dimensions of the drift chambers. For the reconstruction by backward tracking, we exagerated the sizes of the vacuum pipe, the silicon detector and the Pb

target. This is necessary in order to have all the simulated trajectories registered in the detectors, transmited through the pipe and reaching the Pb target.

For the backward tracking case, we included new elements in the simulation. In particular, we have between the two DHC a layer of Pb with a thickness which is half of the target thickness, a layer of silicon equal to the silicon detector and a layer of iron equal to the exit window of the vacuum pipe. We introduced these layers of matter to correct the energy loss. Notice that the deflection of an ion through the magnetic field depends on its energy and we want the simulated protons to enter the dipole with the same energy as the measured ones, otherwise we could not reconstruct properly the momentum.

Moreover, the iron constraints of the magnet are not included in the simulation for the backward tracking reconstruction. This is because the protons touching the iron constraint would loose energy before entering the magnet and this would disturb the momentum reconstruction.

2. *Tracking*
We introduced also some changes in the tracking subroutines. We ignored the energy straggling, the angular straggling and the finite resolution of the detectors. If they were taken into account, we would have to simulate several times each trajectory and we would have to work with the mean value of the positions in the detectors, increasing the time for the reconstruction by a factor of 100.

The other important change is refered to the step size. In this case we did not limit the maximum step size and it was automatically chosen by Geant. The simulation is much more faster and we are not introducing any mistake because the energy loss is still well calculated and Geant selects an appropiate step for the tracking in the magnetic field.

2.3 Results

Although both reconstruction methods can be considered conceptually equivalent, we do not achieve the same resolutions with them. In figure 2.1, we show the results at 500 MeV, for a 200 mg/cm^2 Pb target and with a magnetic field of 1.35 T in the ALADIN dipole. We plotted the magnitude $\frac{\Delta p}{p}$ described in equation 2.2 and we fitted the resulting distribution to a gaussian function. We took as the relative momentum resolutions the values of sigma resulting from the fits, which are respectively 0.61 % and 0.26 % for the forward and the backward tracking methods.

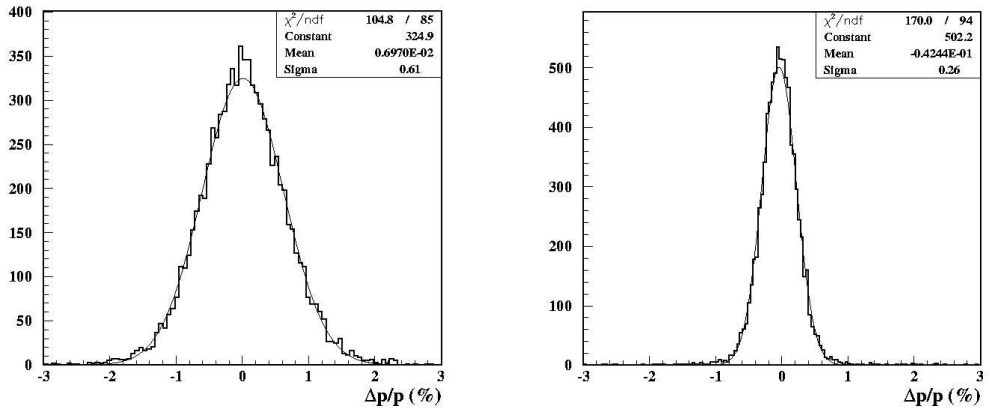

Figure 2.1: *Momentum resolution achieved with the forward (left) and the backward (right) tracking methods. The results correspond to an energy of* 500 MeV *and a* 200 mg/cm^2 *Pb target.*

$$\frac{\Delta p}{p} = \frac{p_{reconstructed} - p_{real}}{p_{real}} \tag{2.2}$$

We found some cases without convergency for the two methods; i.e., cases where it was not posible to find a momentum which reproduced the measured positions. Most of them are related with the big angular straggling suffered by the protons emitted with the biggest angles and touching the iron constraint placed at the exit of the ALADIN magnet. But anyhow, for simulated protons with an angular spread of 0.02 rad (based on the CD distribution at 250 MeV/u) the no convergency cases are not more than a 3 %.

Moreover, when the convergency is reached for the protons touching the iron constraint, we obtain tails in the $\Delta p/p$ distributions. To avoid them, we introduced a cut in the x position registered by the first drift chamber, $x_{DHC1} > 5\ cm$ (in the chamber reference frame). This cut will reduce a bit the efficiency we get.

We see in figure 2.2 the number of needed iterations to achieve the convergency, which is around 10 in most of the cases. This number does not change with the method we use for the momentum reconstruction.

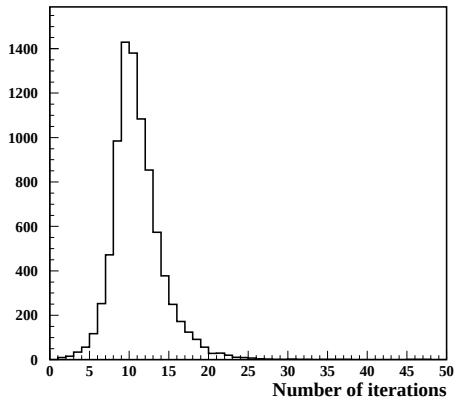

Figure 2.2: *Number of iterations needed for convergency.*

In the following sections we will analize how the momentum resolution depends on different factors as the angular straggling in the elements of the setup, the detector resolutions, the target thickness and the proton energies. Because the results provided by backward tracking are a factor three better than the ones we obtained with forward tracking, we focused our attention in the first method and it was the one we used in most of the cases.

2.4 Contributions to the momentum resolution

We tried to separate the different terms that contribute to the proton momentum resolution. In principle, these contributions come from the interaction with the matter in the setup (mainly the angular straggling) and from the spatial resolution of the tracking detectors.

The simulations were done for 250 MeV protons and a magnetic field inside ALADIN of 0.9 T. In this case, there was not He bag between the two DHC, but air. We used a 200 mg/cm^2 Pb target. Moreover, the step size was automatically chosen by Geant; this means that the effect of the angular straggling was underestimated respect to the real situation and the results should be understood only as a rough evaluation of each contribution.

Firstly, we made a full simulation where everything was taken into account and we reconstructed the proton momentum by backward tracking. We obtained a resolution of $\sigma_T = 0.48$ %. Then, we calculated the different contributions to this number in two ways

1. We made a simulation taking into account all the elements in the setup except the one we wanted to study. We estimated the effect of this element by sustracting quadratically the achieved resolution from the one we obtained when the full simulation was considered.

$$\sigma_k = \sqrt{\sigma_T^2 - \sigma_{T-k}^2} \tag{2.3}$$

2. We only included in the simulation the He within the ALADIN gap and the element we wanted to study. Its contribution is calculated by sustracting quadratically the resolution achieved only with He inside ALADIN from the obtained one[1].

$$\sigma_k = \sqrt{\sigma_{He\ ALADIN+k}^2 - \sigma_{He\ ALADIN}^2} \tag{2.4}$$

We can observe in table 2.1 the results we found. They are surprisely different, mostly for the small contributions and for the value corresponding to the He within the dipole.

Element	σ_1 (%)	σ_2 (%)
Pb target	0.07	0.03
Silicon Strip Detector	0.08	0.02
Fe window of vacuum pipe	0.30	0.28
He inside ALADIN	0.20	0.08
Air in HALL	0.36	0.34
Gas in DHC1	0.17	0.13
Gas in DHC2	0.	0.
Resolution both DHC	0.10	0.05
Mylar both DHC	0.08	0.06

Table 2.1: *Contributions to the proton momentum resolution, they were calculated using the methods* 1 *and* 2.

[1]The time required for the simulations increases when the media in the ALADIN gap is vacuum. This is why we always considered He inside the magnet.

We will add quadratically all the contributions and we will compare the result with the resolution we obtained in the full simulation $\sigma_T = 0.48$ %.

$$\sigma_T = \sqrt{\Sigma_k \sigma_k^2} = \begin{cases} 0.56\ \% & \text{method 1} \\ 0.47\ \% & \text{method 2} \end{cases} \tag{2.5}$$

Even if the results are different for each method, it is clear that the main contribution comes from the angular straggling in the air surrounding the setup. Considering this, we decided to place the He bag between the drift chambers, looking for an improvement of our results.

We did not see any change in the resolution in a first try after including the He bag. The reason was that we were using the Geant automatic steps for the simulations. The effect that the angular straggling in the air between the chambers would have on the proton positions registered by the second chamber was not taken into account because the tracking between the DHC was made in only one step.

However, when we limited the step size we found the improvement we were looking for. We obtained resolutions of 0.47 % and 0.61 % with and without the He bag. Notice that the result with the He bag is the same to the one achieved without the bag but using the automatic step size. In the first case, the effect of the angular straggling in the He between the chambers is well reproduced but it is very small and in the second case, the effect of the straggling in the air is not considered.

2.5 Effect of the Pb target thickness in the momentum resolution

It is necessary to determine the optimum thickness of the Pb target for the ^{23}Al coulomb dissociation. It should be as thick as posible in order to increase the probability of reaction in the target and it should be thin enough in order not to disturb the momentum reconstruction.

Our purpose was to evaluate the thickness which fulfills both requeriments. We studied the relative momentum resolution considering several Pb target thickness; in particular 200 mg/cm^2, 500 mg/cm^2 and 1000 mg/cm^2.

$\sigma_{p,forward\,tracking}$ (%)	$\sigma_{p,backward\,tracking}$ (%)	thickness (mg/cm^2)
0.616	0.264	200.
0.618	0.274	500.
0.627	0.276	1000.

Table 2.2: *Relative momentum resolution for different Pb target thickness.*

$\left(\frac{\Delta p}{p}\right)_{mean\,value}$ (%)	*thickness* (mg/cm^2)
-0.05	200.
-0.07	500.
-0.12	1000.

Table 2.3: *Mean value of the $\Delta p/p$ distribution for different Pb target thickness.*

The results achieved with the two methods of reconstruction are shown in table 2.2. We see that the thickness has not a relevant contribution to the momentum resolution. We only observed the effect of the target using the backward tracking method without introducing the layer of lead between the two drift chambers in the simulations for the reconstruction [2]. In such a situation, there is no correction for the energy loss before the entrance in the magnet and the mean value of the $\Delta p/p$ distribution moved slightly from zero to negative values when we increased the target thickness (see table 2.3).

We can clearly see this effect when we simulate protons in the ALADIN setup and we switch off all the realistic effects, remaining only the interaction with the matter in the target and the location straggling for the emission point. The results are plotted in figure 2.3, where we see that the momentum is underestimated because of the energy loss in the target, depending on the longitudinal coordinate z of the emission point. When we reconstruct the momentum introducing the layers of matter between the drift chambers, the energy loss is taken into account and the distributions shown in figure 2.3 are centered at zero.

We will select a 500 mg/cm^2 target for the rest of our work. We risk to spoil the reconstruction of the emission angles if we use 1000 mg/cm^2.

[2] In the simulations, the layers of silicon and iron between the two DHC were also removed.

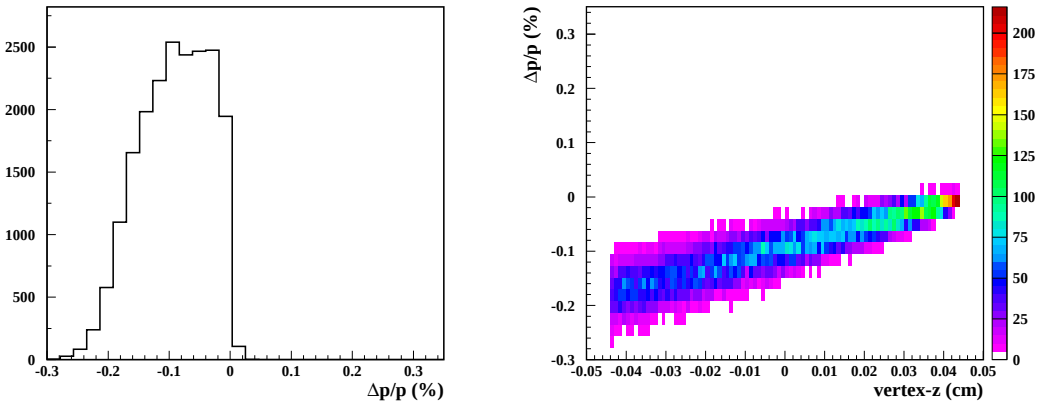

Figure 2.3: *$\Delta p/p$ distribution (left). $\Delta p/p$ versus z coordinate of the emission point in the target (right). The simulations were done for protons at* 500 MeV *and with a* 1000 mg/cm^2 *target; only the location straggling and the interaction with the matter in the target were considered.*

2.6 Relation between the resolution and the proton energy

We considered three different energies for protons, 250 MeV, 400 MeV and 500 MeV. The magnetic field was increased proportionally to the proton momentum (see equation 1.5), in order to preserve the deflection angle, which was 31 deg.

We made the simulations using the Geant automatic step size and we reconstructed the proton momentum only with the backward tracking method. The results are shown in table 2.4; as it was expected, there is an improvement of the resolution for highger energies because the angular straggling is smaller.

We also found that the number of no convergency cases depends on the energy. It is smaller for 250 MeV than for 400 MeV because in the first case protons passing through the iron constraint at the exit of the magnet are stopped and are not detected. When we go to 500 MeV the number of no convergency cases is reduced because the angular straggling is reduced.

Energy (MeV)	B_{ALADIN} (T)	σ_p (%)	No convergency cases (%)
250.	0.9	0.48	2.
400.	1.18	0.32	3.
500.	1.35	0.27	2.

Table 2.4: *Momentum resolution and number of cases without convergency for different proton energies.*

2.7 Results combining the two reconstruction methods

We considered the posibility of estimating the proton momentum combinig both reconstruction methods. The idea was to calculate the proton momentum as the weighted mean value of the results obtained with the forward and the backward tracking procedures. We used the equation 2.6 and the corresponding sigma would be given by equation 2.7.

$$p_{mean} = \frac{p_{forward}\frac{1}{\sigma^2_{forward}} + p_{backward}\frac{1}{\sigma^2_{backward}}}{\frac{1}{\sigma^2_{forward}} + \frac{1}{\sigma^2_{backward}}} \tag{2.6}$$

$$\sigma_{mean} = \left(\frac{1}{\sigma^2_{forward}} + \frac{1}{\sigma^2_{backward}}\right)^{-\frac{1}{2}} \tag{2.7}$$

Considering $\sigma_{forward} = 0.61$ % and $\sigma_{backward} = 0.27$ % (our results at 500 MeV), we predicted a final resolution $\sigma_{mean} = 0.247$ %. However, the resolution we obtained was 0.30 %, see figure 2.4.

The improvement in the resolution would appear if the results achieved with the two methods were disentangled, but in figure 2.4 we show that this is not our case. We have seen that the resolution depends on the method we consider for the reconstruction; but we also know that it is limited by the proton trajectory itself, which suffers the angular straggling in the setup and affects both methods in the same way. For example, if the proton is deviated and goes to a larger position in the first drift chamber, we will underestimate the momentum using both forward and backward tracking. This correlation between the results is the responsible of

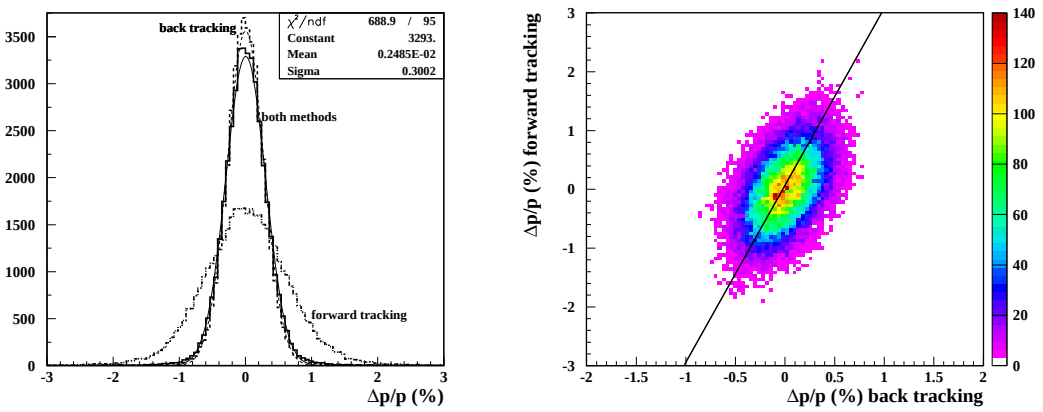

Figure 2.4: *Momentum resolution combining the forward and the backward tracking methods (left). $\Delta p/p$ obtained with forward tracking versus $\Delta p/p$ obtained with backward tracking (right)*

the resolution we obtain combining the two reconstruction methods.

In the next chapter we will only consider the proton momentum reconstruction by the backward tracking procedure.

Chapter 3

Simulations of the ^{23}Al Coulomb Dissociation

We have simulated the ^{23}Al CD at 250 MeV and at 500 MeV using the corresponding event generator. The proton momentum resolutions agreed to the ones given in table 2.4 and the number of no convergency cases was reduced to zero at 500 MeV. Remember that in the previous chapter we always worked with a proton angular aperture of 0.02 rad, based on the CD distribution at 250 MeV. However, the proton emission is more focused forward when we increase the energy and only few of them will touch the iron constraint at the exit of the ALADIN magnet.

We have evaluated the geometric efficiency we expect for the CD experiment. We will also show the position distributions in the detectors and the reconstruction of the invariant mass and the scattering angle in the CD reaction. In principle, we only took into account the feeding of the 0^+ ground state of ^{22}Mg; the feeding of the 2^+ state will be considered in the last section of the chapter.

3.1 Geometric efficiency

The geometric efficiency ϵ_{geom} is limited by the protons. In figure 3.1, we see that they are emitted with an angular aperture four times bigger than the ^{22}Mg ions and they also suffer a larger deflection in the ALADIN magnetic field.

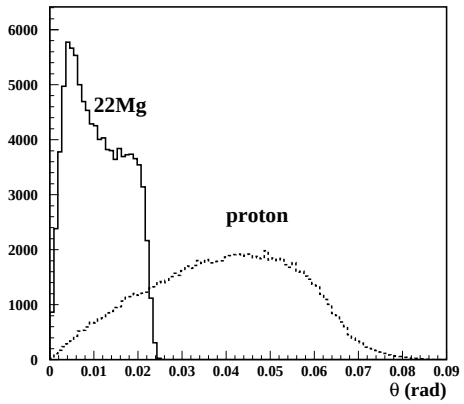

Figure 3.1: *Distribution of the θ emission angle for the protons and the ^{22}Mg produced in the ^{23}Al coulomb dissociation at* 500 MeV/u.

The need of a reasonable efficiency for the experiment forced us to place the drift chambers as close as posible to the magnet. The chambers can not stay centered in the proton trajectories because they could be reached by the ^{22}Mg ions and be damaged; to avoid this problem we moved the detectors to the right side (see figure 1.1).

As we already said, the proton angular aperture is reduced when we increase the energy and this will improve the geometric efficiency. In table 3.1 we summarize the results at 250 MeV/u and at 500 MeV/u. The second numbers we write for 500 MeV/u correspond to a different position of the second DHC, which is closer to the center of the proton trajectories.

Energy (MeV/u)	Fragment	ϵ_{geom} (%)
250.	^{22}Mg	77.
	proton	55.
	both	41.
500.	^{22}Mg	97./ 100.
	proton	87./ 89.
	both	85./ 89.

Table 3.1: *Geometric efficiency in the ^{23}Al coulomb dissociation.*

These numbers suggest to increase the energy up to 500 MeV/u in order to get a good efficiency. We should also remember that we introduced a cut for the proton positions in the first DHC. This cut excludes the protons which touched the iron constraint at the exit of the dipole and reduces a bit the efficiency; from 89 % to 84 %.

3.2 Positions in the detectors

It could be useful to know the position distributions for the ^{22}Mg in the GFI detectors and for the protons in the DHC. They are shown in figure 3.2 for the CD at 500 MeV/u, where the sizes of the frames correspond to the dimensions of the detector active areas.

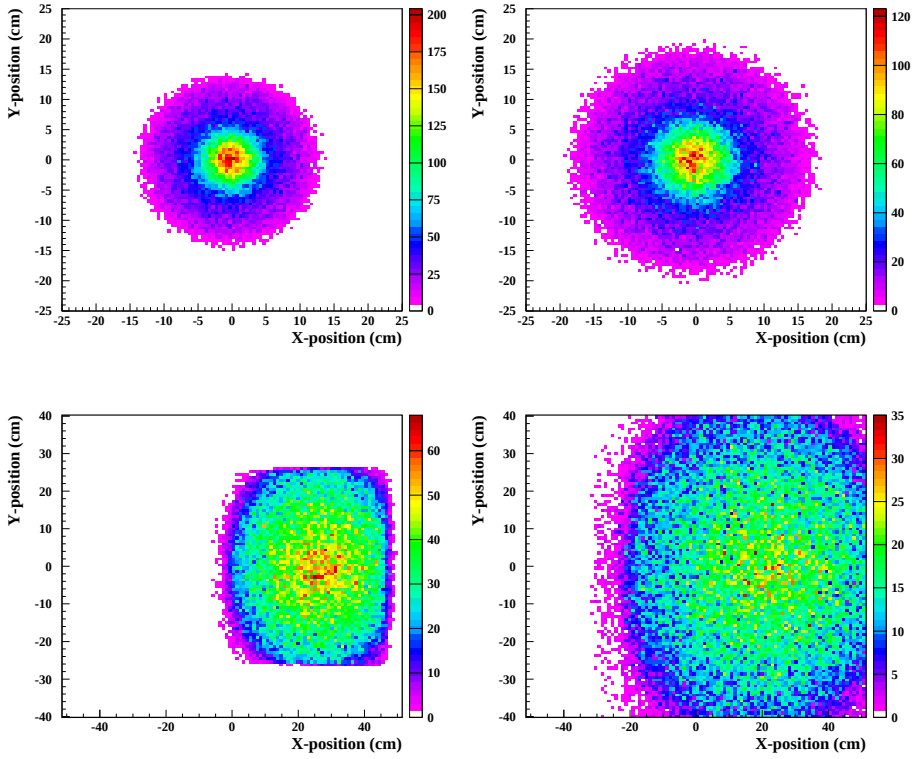

Figure 3.2: *On the top we have the position distributions of the ^{22}Mg ions in the first (left) and the second (right) GFI detectors. On the botton, idem for the protons in the DHC.*

The vertical cuts we see in the position distribution at the first DHC are due to protons which have not been registered by the silicon detector or which have not been transmitted through the vacuum pipe or the ALADIN magnet.

3.3 Relative energy and scattering angle reconstruction

Once we have reconstructed the proton momentum and the θ and ϕ emission angles for the protons and the ^{22}Mg, we can calculate the relative kinetic energy between the fragments and the scattering angle of the CD reaction. The relative kinetic energy in the center of mass is related with the invariant mass M by the equation 3.1.

$$E_{rel} = M - (M_p + M_{^{22}Mg}) \tag{3.1}$$

where

$$M = \sqrt{(E_p + E_{^{22}Mg})^2 - \sum_{i=x,y,z} (P_{i,p} + P_{i,^{22}Mg})^2} \tag{3.2}$$

E_p and $E_{^{22}Mg}$ are the total energies of the proton and the ^{22}Mg and P_i are the different momentum components, all of them in the laboratory reference frame.

For the proton, the momentum reconstruction gives us the momentum magnitude, which is used to calculate the energy E_p and also the momentum components when we determine the emission angles.

In the case of the ^{22}Mg, it makes no sense to reconstruct the momentum because the width of the momentum distribution is comparable to the resolution we expect [14]. This narrow distribution is shown in figure 3.3 and allows us to make an approximation and use its central value, corresponding to the ^{23}Al energy, as the ^{22}Mg momentum for our calculations.

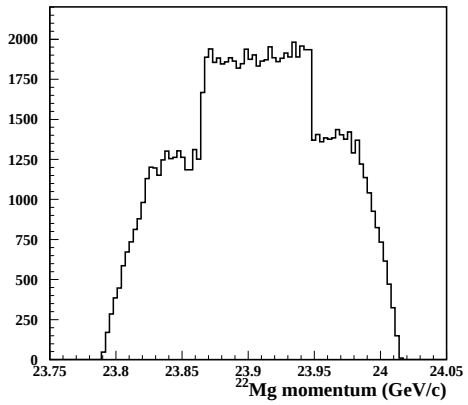

Figure 3.3: ^{22}Mg *momentum distribution in the* ^{23}Al *coulomb dissociation at* 500 MeV/u.

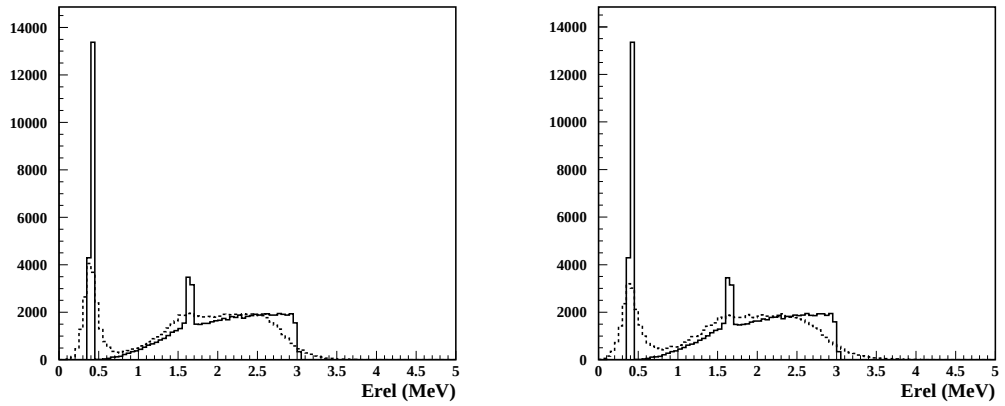

Figure 3.4: *Reconstructed and real* E_{rel} *distributions for the* ^{23}Al *coulomb dissociation at* 500 MeV/u. *On the left side we show the results for a* 500 mg/cm^2 Pb *target and on the right side, for* 1000 mg/cm^2.

We compare the real E_{rel} with the reconstructed one in figure 3.4 for two different target thickness, 500 mg/cm^2 and 1000 mg/cm^2, and we see that the reconstruction is a bit better for the thinner target. We observe two resonances related with the feeding of the 0^+ state in ^{22}Mg, one occurs at 405 KeV and comes from the ^{23}Al first excited state and the other occurs at 1650 KeV and comes from the ^{23}Al second excited state.

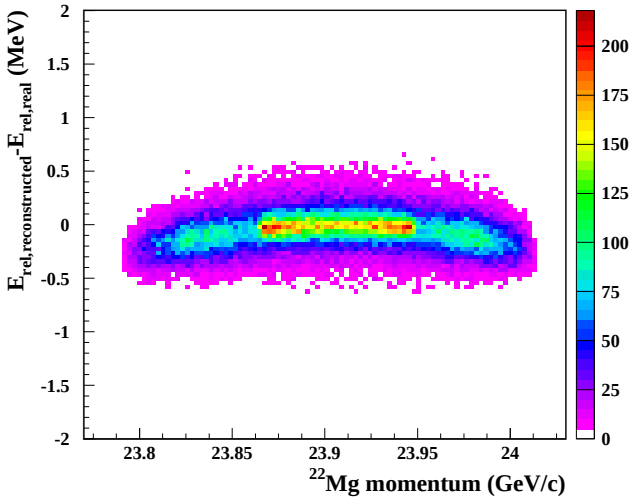

Figure 3.5: *Accuracy of the E_{rel} reconstruction as a function of the ^{22}Mg momentum.*

We have also checked the effect of our aproximation for the ^{22}Mg momentum. We can see it if we plot $\Delta E_{rel} = E_{rel,reconstructed} - E_{rel,real}$ as a function of the real ^{22}Mg momentum in the simulation. The curvature in figure 3.5 shows that we underestimate the relative energy when we go to ^{22}Mg momentums far from the central value, which is the one we used for the calculations. This is because the relative energy and the ^{22}Mg momentum are correlated in such a way that the extremes of the ^{22}Mg momentum distribution correspond to the highest values of the relative energy.

For the scattering angle determination we used the equation 3.3. We present the results in figure 3.6, where we find again that the reconstruction looks slightly better for the 500 mg/cm^2 target.

$$\theta_{scat} = atan\frac{\sqrt{(P_{x,p} + P_{x,^{22}Mg})^2 + (P_{y,p} + P_{y,^{22}Mg})^2}}{P_{z,p} + P_{z,^{22}Mg}} \tag{3.3}$$

The sensitivity of the scattering angle to the momentum of the CD fragments is smaller than the sensitivity of the relative energy [14]. For this reason, we have not studied the error introduced by our approximation for the ^{22}Mg momentum.

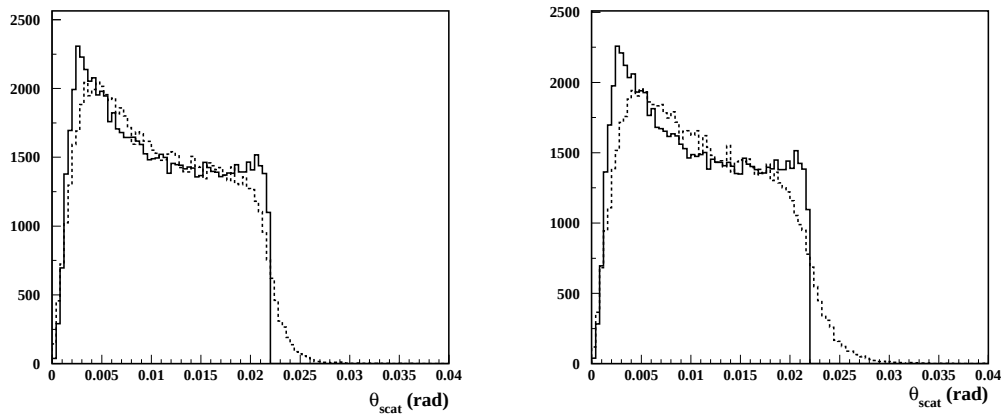

Figure 3.6: *Reconstructed and real distributions of the scattering angle in the ^{23}Al coulomb dissociation at 500 MeV/u. On the left side we show the results for a 500 mg/cm^2 Pb target and on the right side, for 1000 mg/cm^2.*

3.4 The 2^+ state in ^{22}Mg

As it was already mentioned, the results we have presented up to now correspond to ^{23}Al CD simulations where we only considered the feeding of the 0^+ ground state of the ^{22}Mg. The feeding of the 2^+ excited state in ^{22}Mg would come from the ^{23}Al in the second excited state and corresponds to a relative kinetic energy of 404 KeV. It will be identified in the experiment by detecting the γ-rays emitted in the ^{22}Mg decay to the ground state.

As we want a realistic simulation of the experiment, the 2^+ state should be also taken into account. For this purpose, we have created a new input data file with the kinematic parameters of the CD fragments. It contains again 10^5 CD events, but only 0.25 % correspond to the 0^+ case and 0.75 % correspond to the 2^+ case. These percentages were calculated using the respective cross sections, which are 14.55 mb and 43.09 mb for the 0^+ and the 2^+ states (at 500 MeV/u and integrated from $E_{rel} = 0\ MeV$ to $E_{rel} = 3\ MeV$).

In this case, protons are emitted with a larger angular aperture (see figure 3.7) and the simulation showed how the geometric efficiency goes down respect to the single 0^+ results, being $\epsilon_{geom} = 82.73$ %. Moreover, if we apply the cut on the proton position measured by the first DHC, the efficiency decreases to 75.42 %.

In figure 3.8 we present the real and the reconstructed distributions of the relative kinetic energy between the fragments and the scattering angle.

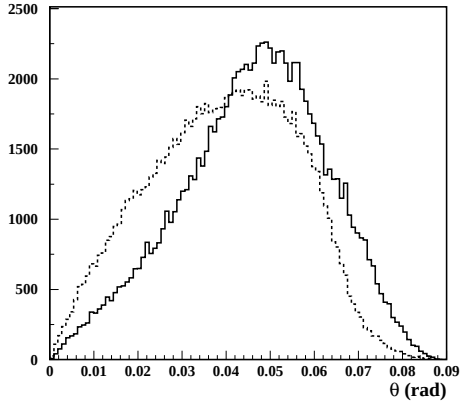

Figure 3.7: *The solid line represents the θ emission angle for the protons when we consider the feeding of the 0^+ and 2^+ states of ^{22}Mg in the ^{23}Al coulomb dissociation at 500 MeV/u. The dashed line corresponds to the distribution when we only consider the 0^+ state.*

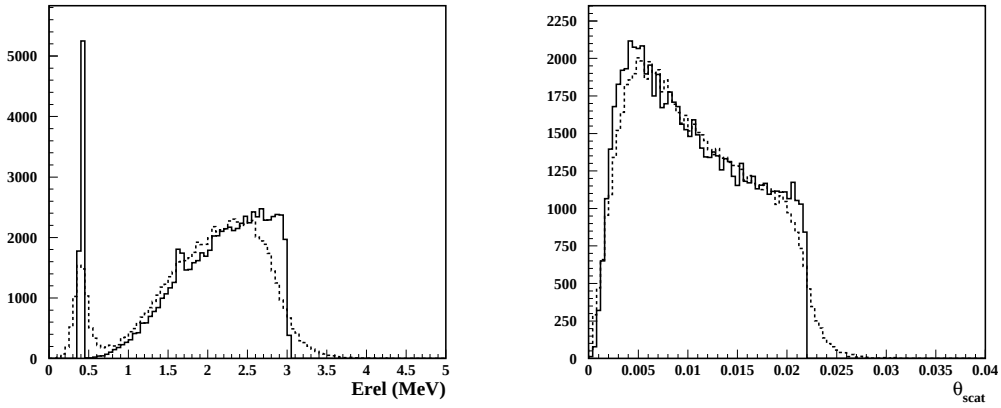

Figure 3.8: *The plot on the left side shows the real (solid line) and the reconstructed (dashed line) distributions of the relative kinetic energy between the fragments for the ^{23}Al coulomb dissociation at 500 MeV/u and a 500 mg/cm^2 Pb target. On the right side, idem for the scattering angle distribution. The simulations were done considering the posibility of feeding the 0^+ and the 2^+ states of ^{22}Mg in the reaction.*

Conclusions

The main purpose of this work was to define the energy for the ^{23}Al CD reaction and to fix the different elements of the setup which will be used for the future experiment; i.e., the Pb target thickness, the location of the tracking detectors, etc.

We have performed an accurate simulation of the ALADIN setup using the software package Geant 3.21, where we reproduced the behavoir of the ^{22}Mg and protons produced in the ^{23}Al CD. It is necessary to determine the proton momentum in order to calculate the relative energy between the fragments and the scattering angle of the reaction; we have developed two methods for the proton momentum reconstruction, called forward and backward tracking. The principal requirements were the velocity, the flexibility and a reasonable resolution; the first and the second ones are fundamental if we want to study how the proton momentum resolution is affected by the different experimental factors.

Both methods of reconstruction are based on the same idea, we simulate several trajectories for different proton momentums and we look for the one which reproduces the positions we have measured. However, the results achieved by backward tracking are a factor three better than what we obtained using the forward tracking procedure and we have decided to use the first method for the proton momentum reconstruction, which gives a relative resolution of 0.27 % at 500 MeV/u for a 500 mg/cm^2 Pb target.

We have found that the main contribution to the resolution comes from the angular straggling in the air surrounding the setup and we have included an He bag between the two drift chambers DHC in order to improve the results. We have also considered several thickness of the Pb target, 200 mg/cm^2, 500 mg/cm^2 and 1000 mg/cm^2, and we have not observed any significant effect on the proton momentum resolution due to this factor. Nevertheless, the thickness also affects the determination of the emission angles for the fragments and the reconstruction of the

relative energy and the scattering angle. This has pushed to choose the 500 mg/cm^2 target.

When we increase the energy of the reaction, the angular straggling is reduced and the proton momentum resolution becomes better. The difference between the resolution at 250 MeV/u and at 500 MeV/u is almost a factor two.

Anyhow, there is another point we should consider if we want to decide on the optimum energy for the reaction, the geometric efficiency. When we go to higher energies, the emitted protons are more focused forward and the efficiency improves significantly. Our simulations show that we need an energy of 500 MeV/u to get an efficiency of 84 % or 75 % [1], depending on whether we consider only the 0^+ state of ^{22}Mg or we also include the 2^+ state.

Finally, for the location of the tracking detectors, the drift chambers of the protons were the key point. We did not have any flexibility about it, they should be as close as posible to the magnet, otherwise the efficiency goes down. This fact forced us to move the chambers from the center of the proton trajectories in order not to be touched by the ^{22}Mg ions.

[1] We are taking into account the cut we introduced for the proton positions in the first drift chamber.

Acknowledgments

I would like to thank:

My supervisor D.Cortina for giving me the oportunity of working and learning about nuclear physics. K.Süemmerer for his valuable indications and for his attention during my stay at GSI. C.Sfientti, who provided me the ALADIN field maps and who taught me how to use them. S.Typel, who produced the input data files for the ^{23}Al CD simulations. C.Wimmer, who gave me precise information about the GFI detectors. M.Fernández, who answered my daily questions and who helped me each time I had a problem with the computer, together with D.Pérez, and H.Álvarez. J.Pereira, who helped me when nothing worked at the begining. D.González, for the discussions about some of the results and M.Caamaño, who helped me to understand some of the results and who also answered my daily questions.

Bibliography

[1] T.Gomi *et al.*, Nuclear Physics A, Volume 758, p.761-764 (2005)

[2] http://integral.esac.esa.int/integral.html

[3] http://wwwgro.unh.edu/comptel/

[4] I.Iyundin *et al.*,Astron. Astroph. 300, 422 (1995)

[5] J.A. Caggiano *et al.*, Phys. Rev. C 64 025802 (2001)

[6] G.Baur, C.C.Bertulani, H.Rebel, Nuclear Physics A 548 188 (1986)

[7] http://www.gsi.de

[8] http://cernlib.web.cern.ch/cernlib/

[9] M.Fernández, diploma thesis, University of Santiago de Compostela (2002)

[10] E.Halnet, PhD Thesis, TU Darmstadt

[11] K.-H.Schmidt,E.Halnet,H.Geissel,G.Muenzerberg,J.P.Dufour,Nucl.Instrum.and Methods A260 (1987) 287-303

[12] http://www-linux.gsi.de/ weick/atima/

[13] P.Adrich, Some notes about the motion of the charge particle through the field of a dipole magnet and the mass measurement with the magnetic spectrometer ALADIN, internal document (2002)

[14] C.Rodríguez, diploma thesis, University of Santiago de Compostela (2005)